Limnol. Oceanogr., 43(8), 1998, 1932–1937

Predicting the signal of O_2 microsensors from physical dimensions, temperature, salinity, and O_2 concentration

Abstract—The signal of Clark-type oxygen sensors is controlled not only by the oxygen concentration but also by sensor dimensions, temperature, and salinity. We have developed a mathematical model that predicts the O_2 microsensor signal as a function of these parameters. The only model variable, membrane permeability, can be determined by a one-point calibration; hence, the model can be used for calibrating the signal measured under any temperature and salinity. The model describes the oxygen concentration profile through the sensor and thus allows optimization of sensor construction with respect to stirring sensitivity, signal-to-noise ratio, and response time. The model is demonstrated using oxygen water column profiles off the coast of central Chile.

Oxygen microsensors have been used under conditions with fluctuating temperature (Revsbech and Ward 1984), in temperature and salinity gradients (Gundersen et al. 1992), and for hydrographic measurements because of their extremely short response time (Oldham 1994). Such applications call for a quantitative understanding of signal dependence on changes in salinity and temperature and of a corresponding calibration equation.

The required model is based on the geometry of a cylindrical microsensor tip (Fig. 1). Parameters and variables are presented in Table 1. Oxygen diffuses from the tip of the sensor through the membrane and the electrolyte to the cathode, where it is reduced by consuming four electrons per oxygen molecule. The oxygen concentration at the cathode surface is assumed to be zero, which is a realistic asumption since the cathode surface is capable of reducing much more oxygen than actually enters the sensor under normal working conditions. The oxygen concentrations at the sensor tip ($C_{2,w}$) and in the water far away from the sensor (C_w) are assumed to be identical (i.e., no concentration gradient in the external medium, outside the sensor). The microsensor signal (I) is defined as the sensor output minus the zero-current.

The oxygen flux through the membrane is given by the membrane permeability (i.e., the transport coefficient of the membrane) multiplied by the change in partial pressure over the membrane, divided by its thickness (Crank 1983):

$$F_m = \Psi \frac{(\Delta p_m)}{Z_m}. \tag{1}$$

As the oxygen partial pressure is equal to the oxygen concentration divided by the oxygen solubility,

$$p = \frac{C}{S}, \tag{2}$$

and as the partial pressure is continuous across the membrane–liquid interface, we can rewrite Eq. 1 as

$$F_m = \Psi \left(\frac{C_{2,w}}{S_w} - \frac{C_{1,e}}{S_e} \right) \frac{1}{Z_m}. \tag{3}$$

The oxygen flux through the electrolyte is given by the product of the diffusion coefficient and the concentration change in the electrolyte, divided by the diffusion distance in the electrolyte (Crank 1983):

$$F_e = D_e \frac{C_{1,e}}{Z_e}. \tag{4}$$

Due to conservation of mass, the oxygen flux through membrane and electrolyte must be equal, making it possible to isolate $C_{1,e}$ from Eqs. 3 and 4. The oxygen signal, I, of the sensor, defined as the output minus the zero-current, can be expressed as the oxygen flux through the electrolyte, F_e, multiplied by the area through which the flux is passing (πr^2) and the current generated per mole oxygen reduced, Φ:

$$I = \Phi \pi r^2 F_e = \Phi \pi r^2 p_{2,w} \left(\frac{Z_m}{\Psi} + \frac{Z_e}{D_e S_e} \right)^{-1}. \tag{5}$$

The current generated per mole of oxygen reduced, Φ, was calculated as four electrons per oxygen molecule times the elementary charge times Avogadro's number; i.e.,

$$\begin{aligned} \Phi &= (4 \text{ electron molecule}^{-1})(1.602189 \times 10^{-19} \text{ A s electron}^{-1}) \\ &\quad \times (6.023 \times 10^{23} \text{ molecule M}^{-1}) \\ &= 3.86 \times 10^5 \text{ A s M}^{-1}. \end{aligned}$$

The physical dimensions: r, Z_e, and Z_m were measured under a microscope before the sensor was filled with electrolyte. The solubility, S, under different salinities and temperatures was calculated from Garcia and Gordon (1992). The partial pressure, P, was calculated as the oxygen concentration outside the sensor (Winkler titration) divided by the solubility, as in Eq. 2. The permeability, Ψ, of the silicone used for the sensor membranes (Silastic, Dow Corning) has been reported to be 41.6×10^{-12} M s^{-1} cm^{-1} bar (air pressure)$^{-1}$ (Brautigam et al. 1985). Yasuda and Stone (1966) showed, however, that this value varies by a factor 6, i.e., between 4.82 and 29.0×10^{-12} M s^{-1} cm^{-1} bar (air pressure)$^{-1}$, depending on the degree of hydration of the silicone. Therefore, we calculated the membrane permeability, using Eq. 5, for a relatively large oxygen sensor in order to minimize uncertainties in measured dimensions, in particular, the internal diameters.

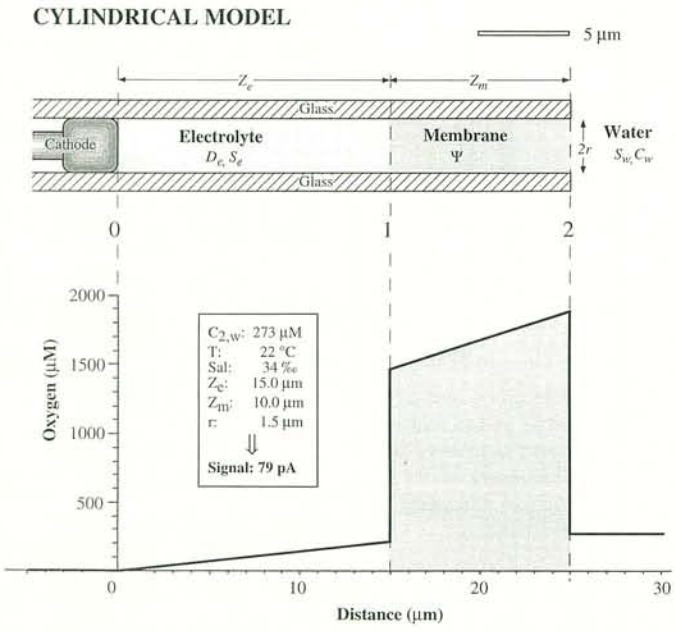

Fig. 1. The idealized sensor tip for the cylindrical model. The physical dimensions, the external conditions, the resulting oxygen concentration gradient through the sensor tip, and the signal are all indicated. (The reason for the sharp discontinuities in the oxygen concentration profile passing over the membrane surface is the much higher oxygen solubility in the silicone membrane.)

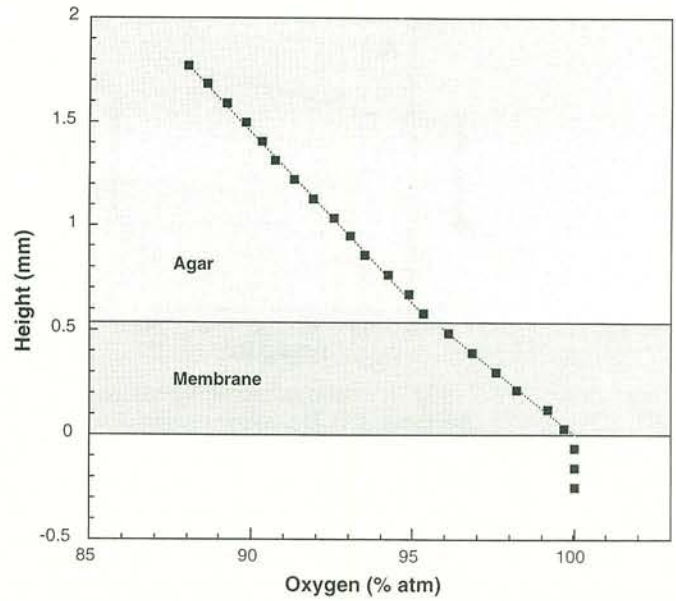

Fig. 2. Gradient in oxygen partial pressure through a silicone membrane and overlying agar measured by a microsensor.

We used the resulting value, 11.19×10^{-12} M s^{-1} cm^{-1} bar (air pressure)$^{-1}$, in testing our model.

We have also determined the permeability of the silicone independently in a diffusion chamber. Specially, a 0.5-mm thick silicone membrane was molded and positioned above a glass chamber that was continuously flushed with pure oxygen. A layer of 1% agar (approximately 7 mm thick) was poured over the membrane, and the system was allowed to equilibrate for 10 h. The oxygen partial pressure through agar and membrane was measured with a microsensor (Fig. 2). At steady state, the oxygen flux (permeability times gradient in partial pressure) through membrane and agar must be equal, as required by mass conservation. As the difference in oxygen permeability of 1% agar and stagnant water is insignificant (Revsbech 1989*b*), we calculated the permeability of the silicone membrane from the oxygen partial pressure gradients in the agar and the silicone, respectively, to be 78% of the permeability of water, or 4.88×10^{-12} M s^{-1} cm^{-1} atm(air)$^{-1}$. This value is about 50% of the value calculated from experimental data and Eq. 5. The discrepancy is probably the result of differences in hydration (Yasuda and Stone 1966) and of an uneven hardening and dehydration of the 1,000-fold more voluminous silicone layer (Fig. 2), as compared with a microsensor membrane. In addition, the permeability decreases over time, probably from precipitation of salts within the membrane or from further hardening of the membrane. These two effects are probably

Table 1. Parameters and variables used in the model.

Symbols	Description	Units	Depending upon
C	O_2 concentration	M l^{-1}	—
D	O_2 diffusion coefficient	m^2 s^{-1}	Temperature, salinity
I	Electrode signal	A	S, D, C, Ψ, r, Z
Φ	Generated current per mole O_2 molecules reduced	A s M^{-1}	—
p	Partial O_2 pressure	atm	C, S
r	Radius of sensing tip	m	—
S	Solubility of O_2	M l^{-1} atm^{-1}	Temperature, salinity
Ψ	Membrane permeability	M m^{-1} atm^{-1} s^{-1}	Temperature
Z	Length	m	—

Indices	Description	Indices	Description
0	Location 0	e	Related to the electrolyte
1	Location 1	m	Related to the membrane
2	Location 2	w	Related to ambient water

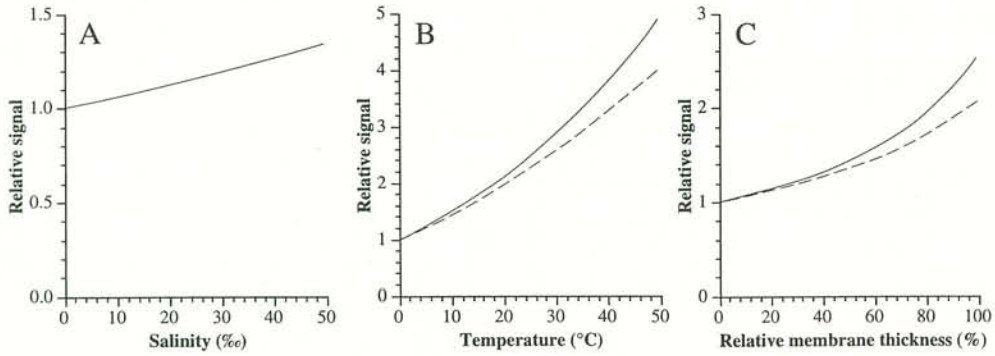

Fig. 3. Relative signal dependence on (A) salinity, (B) temperature, and (C) relative membrane thickness. (A) The salinity-induced signal increase is independent of the relative membrane thickness. (B) The temperature-induced signal increase depends upon the relative membrane thickness. The solid and the dashed lines indicate relative membrane thicknesses of 99.9 and 0.1%, respectively. (C) The relative signal as a function of relative membrane thickness. The solid and the dashed lines indicate signal dependencies at 50 and 0°C, respectively.

responsible for the scatter of data in Fig. 5B. The dependence of temperature on membrane permeability, exp (−1,096/T [absolute temperature]), was taken from Brautigam (1985). The diffusion coefficient, D, at 20°C, 1 atm, in freshwater, was taken from Broecker and Peng (1974) and recalculated to different temperatures and to the salinity of the electrolyte, as described by Li and Gregory (1974).

Equation 5 differs from conventional calibration equations (e.g., Millard 1982) in three ways: (A) it takes diffusion through the electrolyte into account; (B) it predicts the exact signal without variables adjusted upon calibration; and (C) it predicts the oxygen consumption of the electrode.

If Z_e is 0, the signal calculated from Eq. 5 becomes directly proportional to the oxygen partial pressure multiplied by the membrane permeability and divided by the membrane length, in agreement with conventional calibration equations (e.g., Millard 1982). However, in microsensors, Z_e generally contributes significantly to the diffusion distance within the sensor (10–90%); thus, the ratio (Z_e/D_eS_e) must be taken into account. This can be exemplified by modeling the signal response to changes in salinity and temperature. If the oxygen concentration outside the sensor is maintained but the salinity increases, the partial oxygen pressure, p, outside the sensor increases too. As p is the only parameter affected, the signal increases in direct proportion to the partial pressure, independent of the relative membrane thickness, calculated as follows: membrane length divided with the total diffusion length equals $(Z_m/Z_e + Z_m)$ (Fig. 3A). If, in contrast, temperature increases, p and the transport coefficients (Ψ, D) increase, but the oxygen solubility in the electrolyte, S_e, decreases; thus, the larger the relative membrane thickness $(Z_m/Z_e + Z_m)$, the higher is the signal increase (since the last term in the parentheses of Eq. 5 becomes unimportant; Fig. 3B).

The above effect applies to all Clark-type oxygen sensors, because they have an electrolyte phase behind the membrane, but conventional calibration equations do not take this into account. Around 20°C, the signal increases by 4.3% per temperature degree increase for a large relative membrane thickness (99.9%), while for a small relative membrane thickness (0.1%), the signal increase is 4.0% per temperature degree increase. Around 0°C, the signal increases by 3.3% per temperature degree increase for a large relative membrane thickness (99.9%), while for a small relative membrane thickness (0.1%), the signal increase is 2.9% per temperature degree increase. These values are in good agreement with the values of 4–5% per degree reported by Revsbech (1983) for cathode-type electrodes but are somewhat higher than the values of 0.5–1% of the signal per degree reported by Oldham (1994). A large relative membrane thickness results in a higher signal, an effect which is even more pronounced at high temperatures (Fig. 3C).

Most microsensor tips do not have a truly cylindrical shape. Commonly they are conical, and to account for this, an alternative model was derived that takes this into account (Fig. 4). The derivation of this model is more complex, using three-dimensional diffusion in a cone (Crank 1983) instead of linear diffusion in a cylinder. The final signal equation is, however, strikingly simple:

$$I = \Phi \pi r_1 p_{2,w} \left(\frac{Z_m}{r_2 \Psi} + \frac{Z_e}{r_0 D_e S_e} \right)^{-1}. \quad (6)$$

In the special case $r_0 = r_1 = r_2$ (i.e., the sensor tip is cylindrical), Eq. 6 is identical to Eq. 5.

The oxygen concentration gradients through a model sensor with a cylindrical construction are depicted in Fig. 1, and a model sensor with a conical construction is depicted in Fig. 4. The oxygen concentration gradients for the two sensors differ, so despite identical openings (r_2), the conical sensor of Fig. 4 has a signal that is more than three times as high as that of the cylindrical sensor in Fig. 1. The effects illustrated in Fig. 3 are, however, still qualitatively valid.

The signals in picoamperes of 23 oxygen microsensors constructed as described by Revsbech (1989*a*) were recorded and compared to the modeled signals calculated by Eqs. 5 and 6, respectively (Fig. 5). The measured signals varied by a factor of 25, as some of the sensors were constructed specifically to give very high signals (i.e., a short internal diffusion distance combined with a large opening) for valida-

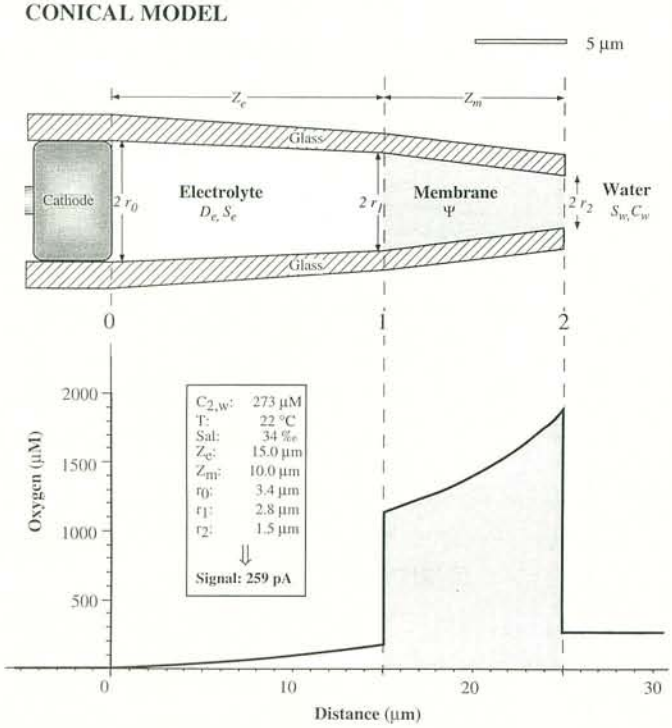

Fig. 4. The electrode tip for the conical model, and Eq. 6. The physical dimensions, the external conditions, the resulting oxygen concentration gradient through the sensor tip, and the signal are indicated.

tion of the model. In contrast to the cylindrical model, Eq. 5, the conical model, Eq. 6, correlates well with the experimental data (Fig. 5). The discrepancy between the cylindrical model and the measured signals is most pronounced for sensors with small signals. The physical explanation is that sensors with small signals generally have a small opening ($2r_2$). The smaller the opening of the sensor, the more the sensor tends to have a conical shape, resulting in an underestimation of the signal by the cylindrical model (Eq. 5). The scatter in data in Fig. 5B is probably the result of differences in membrane permeability and of uncertainty in the measured distances, specifically the internal diameters of the sensors, where a minor error (a fraction of a micrometer) can result in a major error in the modeled signal.

In order to further evaluate the predictions of Eq. 6, we compared the theoretical signal to the experimental signal of a sensor at different temperatures. The signal was recorded with a microsensor with diffusion distances through a membrane (Z_m) and an electrolyte (Z_e) of 7 and 43 μm, respectively. The membrane permeability was determined by a one-point calibration and Eq. 6. Water in a test tube was saturated with atmospheric air at 40°C. The tube was then sealed with a gastight rubber stopper with a penetrating sensor. The temperature was lowered in steps to 0°C, and the readout was recorded after 30 min at each temperature in order to let the water in the test tube reach thermal equilibrium (Fig. 6). The signal predicted by Eq. 6 agrees well with the experimental values.

The exact calibration of oxygen sensors includes the calculation of the oxygen signal, I, as the sensor output minus the zero-current (i.e., the current running in an anoxic environment). The simplest determination of the zero-current is accomplished by adding a little bit of sodium dithionite to a water sample, which results in the instantaneous removal of all oxygen. Most microsensors with a guard cathode (Revsbech 1989a) have zero-currents from 0–2% of the signal in air at laboratory temperature, but some have higher values, which apparently are caused by conductivity and by reducible constituents in the glass (Revsbech pers. comm.). At higher temperatures, the zero-current can contribute significantly to the sensor output (Fig. 6B) and, thus, should always be determined over the temperature interval intended for that sensor.

Additionally, only a one-point calibration for determination of the membrane permeability from Eq. 6 is needed. The oxygen concentration, C, outside the sensor can then be calculated directly by rewriting Eq. 6 using Eq. 2:

$$C = I \cdot S_w \left(\frac{Z_m}{r_2 \Psi} + \frac{Z_e}{r_0 D_e S_e} \right) (\Phi \pi r_1)^{-1}. \qquad (7)$$

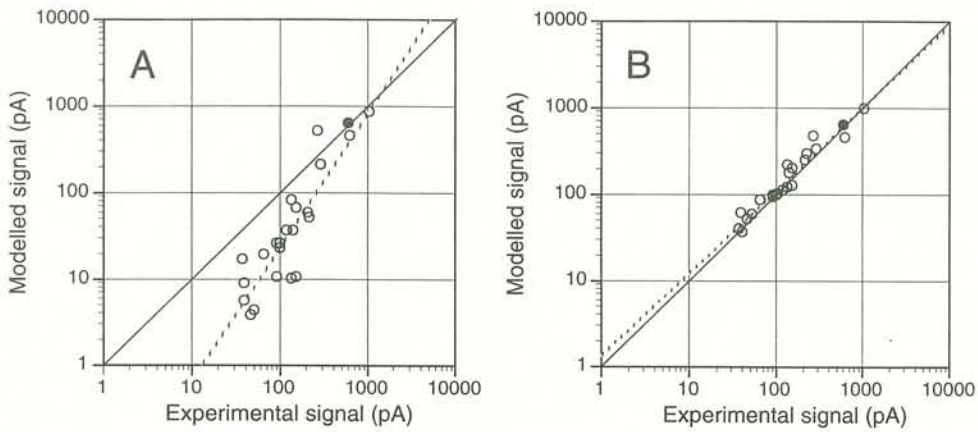

Fig. 5. Modeled signals of 23 oxygen microsensors versus experimentally obtained data. The solid line corresponds to equality of the model and the experimental signals. The dashed line is the best linear fit. (A) Cylindrical model. (B) Conical model.

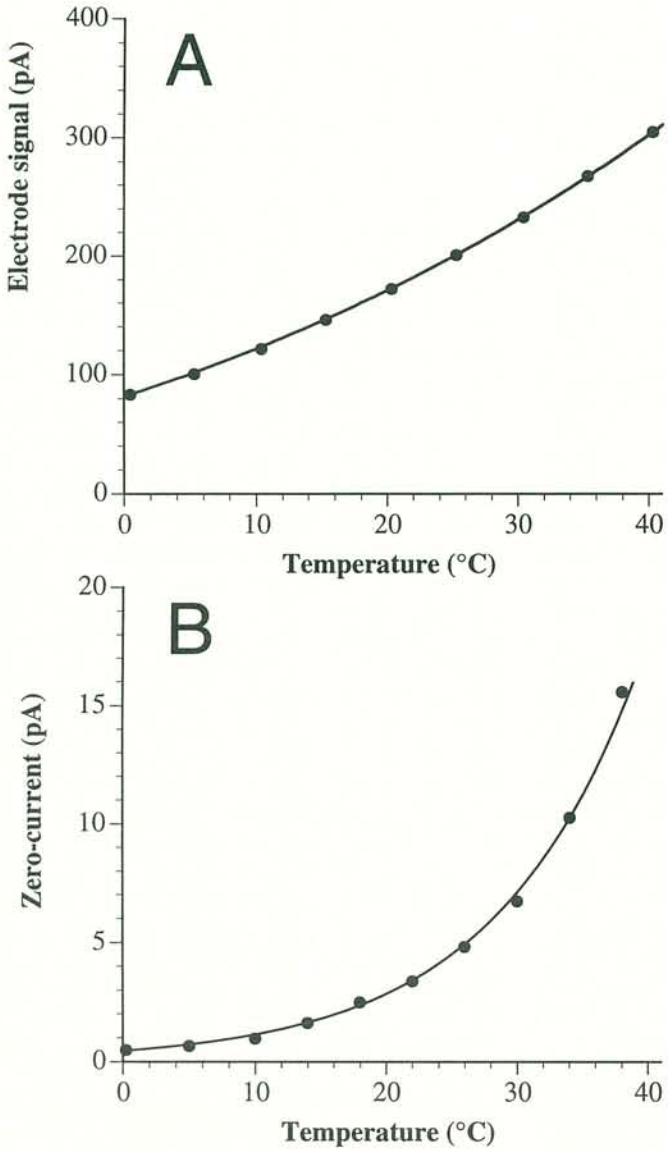

Fig. 6. (A) Temperature dependence of the oxygen signal at constant oxygen concentration (points). Predicted oxygen signal (solid line) as calculated by Eq. 6. (B) The zero-current of an oxygen microsensor versus temperature. Data points are plotted, and the fitted zero-current ($0.4545\ e^{(0.09166\ t)}$, $r = 0.996$) is shown as a line. The zero-current of most microsensors is lower but can be approximated by an exponential equation.

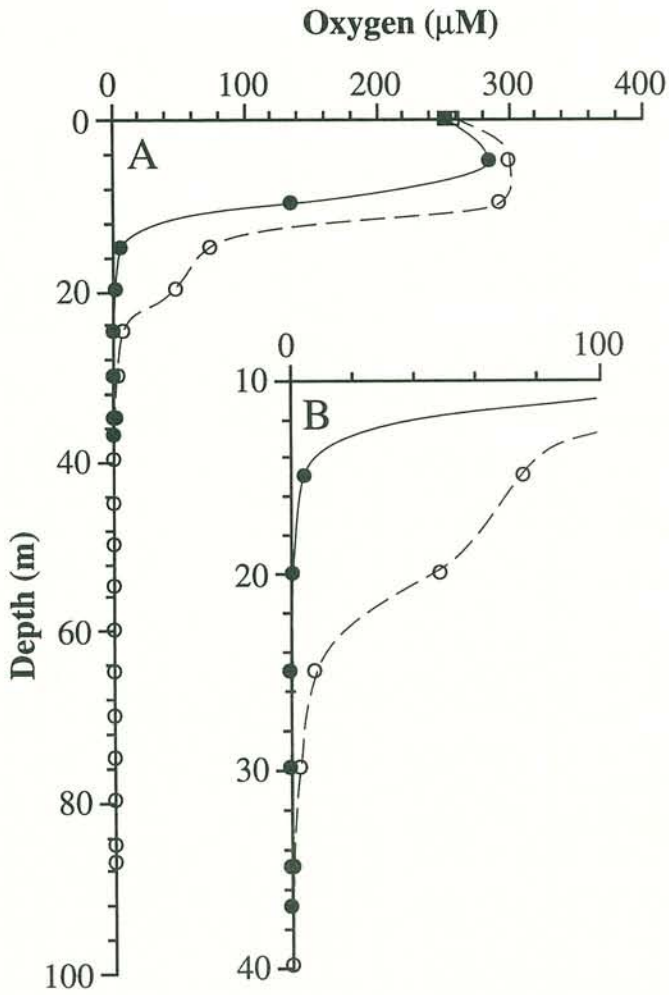

Fig. 7. Oxygen concentration profiles in the water column off Chile, measured at 36°36′5S, 73°00′6W (filled) and 36°25′9S, 73°23′4W in March, 1994. The profiles were measured by lowering an oxygen microsensor mounted on the microsensor instrument Profilur (Gundersen and Jørgensen 1990) in steps of 5 m and subsequently recording the sensor readouts from the instrument. (B) Enlargement of (A). Points indicate the average value of 10 recordings (SD < 0.5%) at each depth after calibration with Eq. 6. The line indicates the fitted oxygen concentration profile.

In stagnant water, a diffusion sphere will be established outside the sensor tip, resulting in a difference between the oxygen concentration at the sensor tip ($C_{2,w}$) and in the ambient water (C_w). This diffusion sphere can be eroded by turbulence, thus resulting in a signal that varies with stirring. The stirring sensitivity can be minimized by constructing the microsensors with a small opening radius r_2 and with a long diffusion path ($Z_m + Z_c$) to the reducing cathode. A tradeoff exists between low stirring sensitivity and short response time, because the response time of sensors increases with the diffusional path. Microsensors can, however, be constructed in such a way that a stirring sensitivity of <1% can be combined with a 90% response time of <1 s (Revsbech 1989a). Therefore, in most cases, the effect of the stirring is negligible. In addition, the ambient water is never stagnant during hydrographic use, which further decreases the difference between ($C_{2,w}$) and (C_w). As a result, no impeller or pump is needed for water column measurements.

One of the advantages of our calibration equation is the higher accuracy obtained in hydrographic measurements. Specifically, measurements are now possible at very low oxygen levels. One example is shown in Fig. 7, where water column oxygen profiles measured off Concepción, Chile, are presented. Because of seasonal upwelling, the primary production is very high, and intense mineralization of organic matter in the water column results in anoxia below 25 and 40 m, respectively, at the two stations. Generally, the terms "low oxygen level" or "below 5 μM" have been used for

deeper waters in this area, because it is difficult to determine these low oxygen concentrations precisely (Fossing et al. 1995). Furthermore, an exact calibration equation such as Eq. 6 is needed when measurements are carried out in environments with high temporal or spatial variations of salinity and/or temperature. Hydrostatic pressure also affects the microsensor signal (Reimers 1987). The combined effect of increasing fugacity (an equivalent to partial pressure) and decreasing membrane permeability (resulting from compression of the membrane) is a near linear decrease to 80% of the signal at 500 bar for a typical microsensor constructed as described here. In this study, the effect of hydrostatic pressure (40 m) is thus about 0.1% of the signal and is considered insignificant. In studies at greater depth, however, hydrostatic pressure must be taken into account.

A more rugged design of the microelectrode has been developed for oxygen measurements in the water phase of benthic chambers (Glud et al. 1995). The sensor has an outside tip diameter of ~1 mm and is thus a minielectrode, but the opening ($2r_2$) through which oxygen enters the electrode is very small (3–20 μm). Therefore, the advantages of a microelectrode are combined with a rugged structure. The oxygen consumption of an oxygen electrode can be of importance when used in small incubation chambers. The oxygen consumption of microelectrodes can be calculated as the signal divided by Φ. Thus, a standard oxygen microsensor with a signal of 79 pA (Fig. 1) consumes 1.7 10^{-8} mM oxygen per day, equivalent to the consumption of all the oxygen in 1 ml of air-saturated seawater (20°C) in 36 yr.

Jens Kristian Gundersen[1]

National Environmental Research Institute
Vejlsøvej 25, DK-8600 Silkeborg, Denmark

Niels Birger Ramsing

Institute for Biological Sciences
University of Aarhus, Denmark

Ronnie Nøhr Glud

Marine Biological Laboratory
University of Copenhagen, Denmark

References

BRAUTIGAM, H. J. 1985. Untersuchungen zum Einsatz von nichtporosen Kunststoff (Siliconkautschuk) Membranen als Sauerstoffeintragungssystem. Hamburger Bericht zur Siedlungswasserwirtschaft.

BROECKER, W. S., AND T. H. PENG. 1974. Gas exchange rates between air and sea. Tellus **26:** 21–34.

CRANK, J. 1983. The mathematics of diffusion. Clarendon.

FOSSING H., AND OTHERS. 1995. Concentration and transport of nitrate by the mat forming sulphur bacterium Thioploca. Nature **374:** 713–715.

GARCIA, H., AND L. I. GORDON. 1992. Oxygen solubility in seawater: Better fitting equations. Limnol. Oceanogr. **37:** 1307–1312.

GLUD, R. N., J. K. GUNDERSEN, B. B. JØRGENSEN, AND N. P. REVSBECH. 1995. Calibration and performance of the stirred chamber from the benthic flux-chamber lander ELINOR. Deep-Sea Res. **42:** 1029–1042.

GUNDERSEN, J. K., AND B. B. JØRGENSEN. 1990. Microstructure of diffusive boundary layers and the oxygen uptake of the sea floor. Nature **345:** 604–607.

———, ———, E. LARSEN, AND H. W. JANNASCH. 1992. Mats of giant sulphur bacteria on deep-sea sediments due to fluctuating hydrothermal flow. Nature **360:** 454–455.

LI, Y. H., AND S. GREGORY. 1974. Diffusion of ions in seawater and deep-sea sediments. Geochim. Cosmochim. Acta **38:** 703–714.

MILLARD, R. C. 1982. CTD calibration and data processing techniques at WHOI using the 1978 practical salinity scale. Proc. Int. STD Conf. Workshop, Mar. Tech. Soc., 19 pp.

OLDHAM, C. 1994. A fast-response oxygen sensor for use on fine-scale and microstructure CTD profiles. Limnol. Oceanogr. **39:** 1959–1966.

REIMERS, C. E. 1987. An *in situ* microprofiling instrument for measuring interfacial pore water gradients: Methods and oxygen profiles from the North Pacific Ocean. Deep-Sea Res. **34:** 2019–2035.

REVSBECH, N. P. 1983. In situ measurement of oxygen profiles of sediments by use of oxygen microsensors. *In* E. Gnaiger and H. Forstner [eds.], Polarographic oxygen sensors: Aquatic and physiological applications. Springer.

———. 1989*a*. An oxygen microsensor with a guard cathode. Limnol. Oceanogr. **34:** 474–478.

———. 1989*b*. Diffusion characteristics of microbial communities determined by use of oxygen microsensors. J. Microbial. Methods. **9:** 111–122.

REVSBECH, N. P., AND D. M. WARD. 1984. Microsensor studies of interstitial water chemistry and photosynthetic activity in a hot spring microbial mat. Appl. Environ. Microbiol. **48:** 270–275.

YASUDA, H., AND W. STONE. 1966. Permeability of polymer membranes to dissolved oxygen. J. Polym. Sci. **4:** 1314–1316.

Received: 27 November 1996
Accepted: 24 March 1998

[1]Corresponding author.

Acknowledgments

We thank Anni Glud, Lars B. Petersen, Anja Eggers, and Unisense ApS for constructing and testing the microsensors. Bo Barker Jørgensen, Niels Peter Revsbech, and Lars Peter Nielsen provided valuable input to the manuscript. This study was supported by the European Commission through MAST Programme contracts 950029 and 970078 and by the Max Planck Society.